J Comp Physiol A (2007) 193:233–247
DOI 10.1007/s00359-006-0185-7

ORIGINAL PAPER

Diverse speed response properties of motion sensitive neurons in the fly's optic lobe

John K. Douglass · Nicholas J. Strausfeld

Received: 16 May 2006 / Revised: 2 October 2006 / Accepted: 7 October 2006 / Published online: 15 November 2006
© Springer-Verlag 2006

Abstract Speed and acceleration are fundamental components of visual motion that animals can use to interpret the world. Behavioral studies have established that insects discriminate speed largely independently of contrast and spatial frequency, and physiological recordings suggest that a subset of premotor descending neurons is in this sense speed-selective. Neural substrates and mechanisms of speed selectivity in insects, however, are unknown. Using blow flies *Phaenicia sericata*, intracellular recordings and dye-fills were obtained from medulla and lobula complex neurons which, though not necessarily speed-selective themselves, are positioned to participate in circuits that produce speed-selectivity in descending neurons. Stimulation with sinusoidally varied grating motion (0–200°/s) provided a range of instantaneous velocities and accelerations. The resulting speed response profiles are indicative of four distinct speed ranges, supporting the hypothesis that the spatiotemporal tuning of mid-level neurons contains sufficient diversity to account for the emergence of speed selectivity at the descending neuron level. This type of mechanism has been proposed to explain speed discrimination in both insects and mammals, but has seemed less likely for insects due to possible constraints on small brains. Two additional recordings are suggestive of acceleration-selectivity, a potentially useful visual capability that is of uncertain functional significance for arthropods.

J. K. Douglass (✉) · N. J. Strausfeld
Arizona Research Laboratories
Division of Neurobiology, 611 Gould-Simpson Bldg.,
University of Arizona, Tucson, AZ 85721, USA
e-mail: jkd@neurobio.arizona.edu

Keywords Vision · Motion processing · Speed discrimination · Acceleration · Insecta

Abbreviations

cpd	Cycles per degree
emd	Elementary motion detector
STF	Spatiotemporal frequency

Introduction

In Newtonian physics, motions of an object or scene relative to an observer can be completely specified by the velocity as a function of time ($V(t)$, incorporating both speed and motion direction), and may also be described by the acceleration (dV/dt). When an animal perceives motion, to what extent are these features faithfully represented in the brain, and how? In visual systems, though individual motion-selective neurons are inherently *responsive* across a range of motion speeds, frequently they are not specifically more selective for changes in speed than in the contrast frequency or spatial frequency content of an input. One consequence is that when presented with motion of a periodic grating stimulus, the responses of an animal or a single neuron depend as much on the temporal frequency (or contrast frequency, the number of grating cycles/s passing a given location within a neuron's receptive field) or the spatial frequency (the number of grating cycles per degree; cpd), as on the angular speed of the grating (°/s). For a periodic grating, these three parameters are related as follows: speed = temporal frequency/spatial frequency. A speed *selective* response is one that is especially sensitive to changes in speed, and relatively insensitive to changes in contrast frequency or spatial frequency (e.g., Priebe et al. 2006).

Previous studies have shown that insects can evaluate visual motion speed. For example, tests of fruit fly (David 1982) and honey bee (Srinivasan et al. 1991) behavior while flying through tunnels show sensitivity to the perceived angular velocity, and relative insensitivity to contrast frequency. Likewise, observations of bee landing responses show that they adjust their flight as if to maintain a constant apparent speed with respect to the landing surface (Srinivasan et al. 1996, 2000). The ability to make speed discriminations like these implies the presence of neural pathways in the visual system which are speed-selective. Indeed, recordings from premotor descending neurons of locust, dragonfly and honey bee (Kien 1975; Olberg 1981; Ibbotson 2001, respectively) show speed selective responses: when stimulated with motion of gratings with fixed spatial frequencies across a range of constant speeds, maximal responses occur near a preferred angular speed instead of a preferred contrast frequency. The underlying circuits that result in speed selectivity, however, are unknown.

In the fly's optic lobe, photoreceptor terminals in the lamina provide the inputs to several parallel pathways that proceed through the medulla to the two deepest retinotopic neuropils, the lobula and lobula plate. These latter neuropils both provide non-retinotopic relays to additional visual processing centers in the lateral deutocerebrum known as optic glomeruli (Strausfeld and Lee 1991), and to descending neurons that supply premotor circuits in the thoracic ganglia. Elementary motion detection is thought to begin at a very peripheral level (Douglass and Strausfeld 2003a; Higgins et al. 2004), where little is known about the speed response properties of motion-sensitive neurons.

Previous recordings from blow fly lobula plate tangential cells (LPTCs) have shown that these elements are selective for the contrast frequency rather than the angular speed of moving gratings. This is consistent with behavioral tests of insect optomotor responses, and studies of mathematically modeled correlation-type motion detectors (Borst and Egelhaaf 1989). When stimulated with gratings having fixed spatial frequencies across a range of speeds, maximal responses of LPTCs occur near a preferred contrast frequency instead of a preferred speed (Eckert 1980). In primates, simple cells in cortical area V1 exhibit similarly unspecialized spatiotemporal frequency (STF) tuning properties, whereas a minority of complex cells in the middle temporal area (MT), which receives major inputs from V1, are speed-selective (Perrone and Thiele 2001; Priebe et al. 2006).

One hypothesis for how visual interneurons acquire speed selectivity involves integrating the activity of otherwise unspecialized motion-sensitive neurons that have distinct, but overlapping STF tunings, as modeled by Grzywacz and Yuille (1990). This type of mechanism, hereafter referred to as the "multiple STF range" hypothesis, seems easily feasible for large-brained animals that possess many motion-sensitive neurons with distinct STF tunings, but is arguably less likely in insects (Higgins 2004) because constraints on brain size may limit how many neurons can be devoted to such a circuit (Streidter 2005). Though interspecific differences in STF tunings have been discovered which are correlated to visual ecology (O'Carroll et al. 1996), intraspecific analyses to date have failed to suggest the presence of more than two distinct STF tunings within an individual (e.g., Horridge and Marcelja 1992; O'Carroll et al. 1997).

Alternatively, speed selectivity could arise much more peripherally as an inherent property of elementary motion detector (emd) circuits. Studies of theoretical Hassenstein–Reichardt (HR) correlators (Hassenstein and Reichardt 1956) show that speed-selective activity can result if the gains at the outputs of each half of a mirror-symmetrical HR emd are unequal (Zanker et al. 1999), or by positing a non-directional variant of this type of circuit (Higgins 2004). Currently, at least with regard to insects, both the multiple STF range hypothesis and emd-based hypotheses suffer from an absence of supporting physiological data. A third scenario is provided by responses to movement of wide-field natural images, which share a certain degree of self-similarity in that they typically contain a mixture of spatial frequencies (f) with an approximately $1/f^2$ power spectral characteristic (cf. van Hateren 1997). The summed responses of arrays of unspecialized model HR correlators (Dror et al. 2001), as well as actual wide-field lobula plate tangential neurons (Shoemaker et al. 2005) show consistent velocity tuning responses to a variety of natural scenes. These important observations nonetheless do not explain speed-selective responses to small-field objects or simple grating stimuli.

This paper offers a test of the multiple STF range hypothesis as it applies to insects, by examining a group of recordings from identified neurons in the optic lobe of the blow fly, *Phaenicia sericata*. Though these particular neurons are neither expected to belong to a single circuit nor claimed to be speed-selective themselves, they are examples of motion-sensitive cells which are in a position to provide direct or indirect inputs to speed-selective descending neurons. Responses were observed while sinusoidally varying the speed of a constant-spatial-frequency grating. The data reveal multiple speed response ranges that are distinct, yet

overlapping, thus supporting the plausibility of the multiple STF range hypothesis for insects.

Also inherent in a stimulus with sinusoidally varying speeds are changes in acceleration (see Results). We define an acceleration-selective visual response as neural activity that is particularly correlated with the acceleration, rather than speed or directional components of a motion stimulus. Two recordings showed evidence suggestive of acceleration selectivity. Since acceleration sensitivity is consistent with some theoretical predictions yet is not evident in all motion-sensitive neurons, these observations suggest that a subset of motion processing pathways in insects may be specifically concerned with acceleration processing.

Materials and methods

All physiological experiments employed a laboratory colony of the calliphorid fly, *P. sericata*, which is maintained at the Arizona Research Laboratories, Division of Neurobiology. The general methods of fly rearing, computerized visual stimulus presentation, intracellular recordings and histological processing have been described previously (Douglass and Strausfeld 1996, 1998, 2003b).

Stimuli and electrophysiology

Adult flies were positioned with the head 18 cm from the center of a computerized stimulus monitor and the eyes aligned horizontally, providing the fly with a frontal view of the stimulus screen. The body was tilted downward 45° from the head's frontoposterior axis, providing access to the optic lobes upon removing a piece of cuticle from the back of the head. Single neurons were impaled within the medulla, the second optic chiasma, or the lobula complex, using sharp borosilicate or quartz pipettes fabricated with a laser puller (P2000, Sutter Instruments, Novato, CA, USA), backfilled with Lucifer yellow CH (lithium salt, Molecular Probes) and 0.1 to 0.2 M LiCl, and advanced with a micromanipulator (Leica) secured to an aluminum wedge so that the fine advance axis is at a 45° angle from vertical. The raw data from T4, CY2 and H6 neurons were obtained from recordings that were first described in Douglass and Strausfeld (1996), which are analyzed here with regard to speed response profiles. In more recent experiments, manual micropositioning of the pipette has been augmented by a piezoelectric drive (IW-800, Burleigh Instruments, Fishers, NY, USA) that is mounted on the manipulator, aligned with the fine adjustment axis, and configured to advance in rapid 0.5-μm steps.

Visual stimuli were provided by a monochrome monitor equipped with ultra-short persistence phosphors and operated at a 200 Hz horizontal refresh rate (Vision Research Graphics, Durham, NH, USA) (Douglass and Strausfeld 2003b), or a color monitor operated in monochrome mode at a 117 Hz refresh rate (Douglass and Strausfeld 1996). Two photodiodes, with accompanying optics and amplifiers, were configured to record the fast temporal features and the relative intensity changes during presentation of the stimuli described below. One photodiode received an image of a small circular region at the center of the CRT, while the second photodiode monitored a full-field view of the entire screen (80° wide by 62° high at the fly's head).

Directional grating motion stimuli were provided by sinusoidally varying the velocity of a full-screen square-wave grating with a constant spatial frequency (Neurosequence software, Vision Research Graphics). Although a sinusoidal grating would be preferable for its pure spatial frequency content, it was not possible to use sinusoidal gratings due to software limitations when generating full-screen, low-spatial-frequency gratings. For all but one of the recordings that were analyzed to obtain speed response profiles (as well as two additional recordings that showed evidence of acceleration-specific activity), the spatial frequency was 0.126 cpd (equivalent to a grating wavelength or period of 8°/cycle), and the range of grating speeds (either 0–95°/s or 0–200°/s) produced contrast frequencies from 0 to 12 Hz or 0 to 25 Hz, respectively. In one additional recording, a 0.05 cpd (20°/cycle) grating was used instead, and the speed was varied from 0 to 200°/s, yielding contrast frequencies from 0 to 10 Hz.

The grating stimuli were not adjusted for geometric distortions of apparent stimulus speeds and grating dimensions, which arise when viewing a planar surface. Thus, depending on a neuron's receptive field location, apparent grating speeds can be somewhat lower than the nominal values measured at the center of the screen. How much could such discrepancies affect conclusions regarding speed response profiles? Given the fly's position 18 cm from the 218 × 300 mm display, the maximum possible change would be at the corners of the display, with apparent speeds of approximately 0.5 × the nominal speed. This corresponds to a maximum $\log_{10}$ change of only 0.30, or less than 9% of the full speed ranges to be examined here (see Results). Based on information about receptive fields and/or dendritic fields of individual neurons, however, actual discrepancies from the nominal grating speeds were judged to be even smaller (see Results).

Intracellular voltages and stimulus timing signals were amplified, then either stored on VHS tape by using a VCR equipped with a PCM recording adapter (Vetter, 3000A, Regensburg, PA, USA), or digitized online and transferred directly to a PC [Power 1401 interface & Spike 2 software v. 3 and 4, Cambridge Electronic Design (CED), Cambridge, England]. Resting membrane potentials were typical for recordings from fly visual interneurons, and ranged from ca. −10 mV for the tiny T4 neuron to −30 to −45 mV for larger neurons.

Histology, light microscopy and anatomical reconstructions

At the end of each experiment, the recorded cell was injected iontophoretically with Lucifer yellow (Molecular Probes, Eugene, OR, USA) by using a steady 1–3 nA hyperpolarizing current for 1–3 min, and the brain was removed from the head capsule, fixed overnight in 4% formalin in Millonig's buffer at pH 7.2, and processed for embedding and serial sectioning in Spurr's plastic (Douglass and Strausfeld 1996, 2003b). Profiles of stained cells were scanned at 0.5–1.0 μm intervals (depending on magnification) with a confocal epifluorescence microscope equipped with an argon laser (Nikon PCM 2000 or Zeiss LSM 5 Pascal system).

Anatomical relationships between intracellularly stained neurons and the surrounding neuropil architecture were revealed in low-magnification confocal images. Morphologies of filled neurons were then reconstructed from higher-magnification confocal projections of individual serial sections, or the confocal projections from separate plastic sections were merged digitally using Corel Photopaint (Corel, Salinas, CA, USA). Cobalt staining methods (Fig. 1) are described by Strausfeld (1991).

Data analysis

Spike2 v.5 (CED) and custom Spike 2 scripts were used to either obtain spike counts or, for nonspiking neurons, to measure mean voltages. If necessary, voltage traces were digitally filtered to attenuate 60 Hz line noise or low-frequency baseline fluctuations (Spike 2 or Microcal Origin software, OriginLab, Northhampton, MA, USA). Speed response profiles were evaluated by using preferred-direction or preferred-orientation responses, when known, or by averaging responses of a non-direction-selective neuron to multiple directions (see Results for details). The nonparametric Wilcoxon two-sample test (Sokal and Rohlf 1981) was used to test for differences in the speed response properties of neurons. In addition, a Z-statistic for testing the difference between two proportions (Walpole 1974) was used to help evaluate the reliability of responses of one neuron that were correlated with motion acceleration.

As responses to motion speed tend to scale logarithmically, analyses were performed using a $\log_{10}$ scale. For all recordings except those from the bushy T cell T4, this involved dividing each sinusoidal motion sweep into temporal bins that represent equal log-speed increments, then obtaining for each bin either the mean spike rate or the mean voltage change from baseline. Whenever possible, response latencies were estimated from flicker responses (available from all but the LPTCx recording described below), and bin times were increased accordingly for better alignment with the actual neural responses. All latencies were small, however (18–50 ms) relative to the 1,250 ms required for a stationary grating to reach its maximum speed. The above binning method is suitable for analyzing the responses of neurons with sufficiently large receptive fields that the effects of the grating's phase are spatially averaged. This applied to all but one of the present recordings. A modified binning method was required for recordings from the T4 neuron, as its responses were obviously phase-locked, indicative of a receptive field with a diameter comparable to the 8° grating wavelength. Thus, for T4 the latency-adjusted bin limits were defined at successive troughs in the intracellular voltage, yielding one response measurement and mean log speed per grating cycle. As the phase delay in T4's responses was not frequency dependent, no adjustment for this was needed.

Results

The first section below describes a group of recordings that show distinct speed response profiles and little or no evidence of acceleration-specific activity. The second section describes two additional recordings that are suggestive of acceleration specific activity.

Distinct speed response ranges suggest a basis for speed discrimination

Figure 1 illustrates the morphology and motion responses of a large, heterolateral motion-sensitive spiking neuron which has arborizations in both medullae, a cell body above the right lobula, and additional branches in the left lateral deutocerebrum. The impalement location for this neuron (hereafter referred to as HeMe1) was in the left (contralateral)

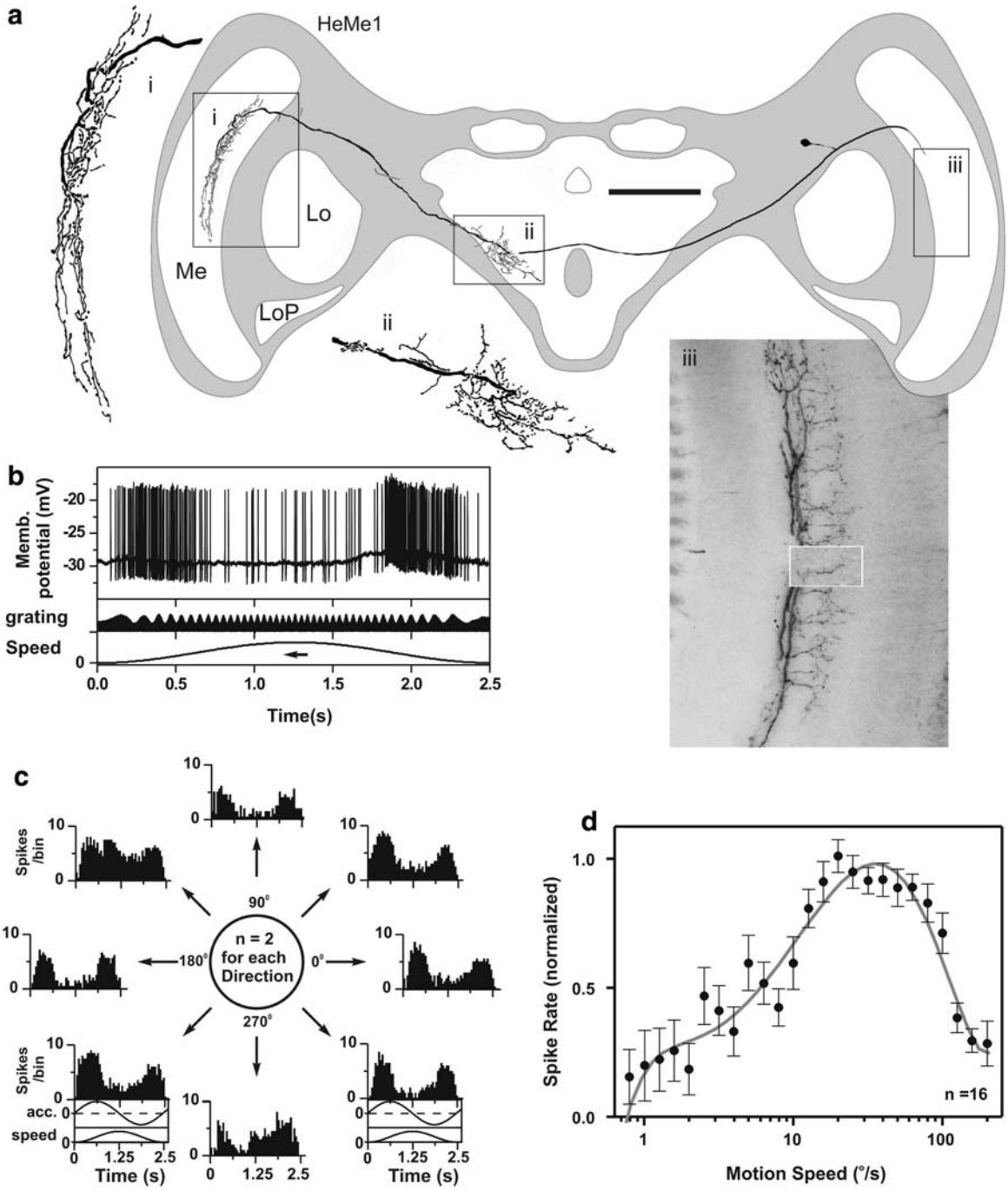

Fig. 1 Morphology and responses of a speed-sensitive, non-direction-selective heterolateral medullary neuron (MeHe1) with extensive tangential arborizations in the inner medulla. **a** Vertical section through brain showing bright staining of terminal arbors in the medulla (*Me*, *inset i*) and in the lateral deutocerebrum (*inset ii*), corresponding to the position of the pipette tip on this side of the brain, near the lobula (*Lo*). Faint ipsilateral staining (*white box within inset iii*) corresponds to short columnar dendritic branches of a medullary neuron that has previously been stained with cobalt (*inset iii*). *LoP*, lobula plate. **b** Example of raw spiking responses (*upper trace*) as the grating motion velocity (*bottom trace*) was varied sinusoidally between 0 and 200°/s (spatial wavelength = 8°; *arrow* indicates leftward motion). Middle trace shows responses of a photodiode to individual stripes traversing the center of the screen. **c** Mean peristimulus time histograms of spike counts (48 ms/bin, $n = 2$ sweeps/direction) while motion velocity was varied sinusoidally as in **b**. The responses demonstrate selectivity for motion speed (*speed*), and not for direction (*arrows*) or acceleration (*acc*). **d** Speed response profile, showing mean spiking activity (± SE) per log speed interval, pooled from the non-direction-selective responses of this neuron to upward, downward, leftward and rightward motion. Smooth curve shows a polynomial fit to the means. *Scale bar* in **a** = 100 μm (applies to main figure only)

optic lobe, in the axonal region just behind the medulla. Whereas arborizations that are close to the impalement site were brightly stained, enough Lucifer yellow diffused into the ipsilateral medulla to reveal a few small columnar branches, such as the one shown boxed in Fig. 1, inset iii. This neuron's distinctive morphology identifies it with a neuron of the same type that was identified in a separate cobalt-stained preparation, a portion which is illustrated in inset iii of Fig. 1. The ipsilateral medulla arborizations of this neuron are characterized by slender columnar dendrites that are equipped with spine-like specializations. The dendritic tree extends across much of the neuropil within deep strata of the outer medulla, where it intersects retinotopic arrays of columnar neurons. The axon extends across the entire brain to the contralateral *inner* medulla (beneath the Cuccati bundle), where it ends with long tangential branches bearing terminal varicosities (Fig. 1i). Thus, HeMe1 connects two different neuropils, the outer medulla being embryologically distinct from the inner (Meinertzhagen and Hanson 1993; Strausfeld 2005). This neuron has an additional projection in posterior dorsal neuropil associated with the terminal regions of wide-field motion sensitive lobula plate neurons (Fig. 1ii).

The background spiking activity of HeMe1 was very low, as is illustrated at the times when sinusoidal motion speeds approached zero (Fig. 1b, c). Spiking activity increased dramatically during grating motion in any direction, and repeated stimulation produced little or no evidence of adaptation to motion. Figure 1b shows a representative intracellular trace obtained during a single 2.5-s period of leftward grating motion, as the speed increased sinusoidally from 0 to 200°/s and then diminished back to 0°/s. Similar traces, obtained during motion in each of eight directions, were used to obtain mean peristimulus histograms of spike rates (Fig. 1c, from a total of 16 traces). Despite variability in overall activity, the responses show a consistent pattern with respect to both motion speed and direction. Whether motion speed was increasing or decreasing, spike rates tended to be maximal at intermediate motion speeds. The only exception to this trend is the response to upward diagonal (135°) motion, in which relatively rapid spiking continued even at high speeds. There is no clear evidence of a preferred motion direction or orientation. In the mean responses to downward (270°) motion the cumulative spiking activity was greater during the latter (decelerating) half of the 2.5 s velocity sweep. Although this discrepancy might be considered suggestive of selectivity for motion deceleration, all of the additional spikes actually occurred during only one sweep, so this was not a consistent feature of the responses.

A speed response profile for this recording was obtained by measuring the spike rate as a function of motion speed (Fig. 1d). As no directional or acceleration/deceleration selectivity was evident, data from the responses to all eight motion directions, and to both acceleration and deceleration, have been pooled. Compared to the nearly zero spike rate in the absence of motion, the HeMe1 neuron showed measureable responses to speeds ranging from approximately 1 to over 100°/s, with maximal responses occurring between approximately 15 and 50°/s.

A neuron that was inhibited rather than excited by the presence of motion is shown in the confocal reconstruction of Fig. 2a, with motion responses in Fig. 2b, c. This is a previously undescribed lobula plate tangential cell (hereafter referred to as LPTCx), the arborizations of which extend across the entire lobula plate. Because the dendritic tree of this cell intercepts all retinotopic afferent bundles to the lobula plate, the inputs to LPTCx subtend the full, roughly hemispherical view of one compound eye. The cell body lies medial to the lobula plate, and a second region of extensive arborizations is found in the lateral deutocerebrum on the same side of the brain. Unlike the arborizations of other lobula plate tangential cells, which tend to be wholly or partially restricted to either the outer, horizontal-motion-sensitive or inner, vertical-motion-sensitive strata, branches of this neuron's dendrites extend from the deepest stratum through the entire depth of the neuropil.

Whereas the HeMe1 neuron showed no activity until stimulated by grating motion, the LPTCx neuron exhibited a high level of background spiking which was inhibited by motion. This is illustrated in Fig. 2b, both at times when the grating motion speed was near zero, and at the end of the third motion cycle, when the grating had become stationary and was replaced by an equiluminant blank screen. In this recording, the background spike rate was initially high but diminished quickly, precluding a detailed quantitative analysis of the response properties. Nonetheless, since the resting membrane potential remained stable and some spiking activity persisted for several minutes (not shown), the rapid initial reduction in spiking activity appears to reflect motion adaptation rather than an early physiological deterioration due to impalement. The initial motion responses of this neuron were used to obtain a speed response profile (Fig. 2c), which shows the spike rate steadily diminishing as motion speeds increased from 0 to 200°/s. Note that if data from subsequent sinusoidal motion sweeps were to be included in the analysis, this would shift the speed response profile to a lower speed range, making the response profile more

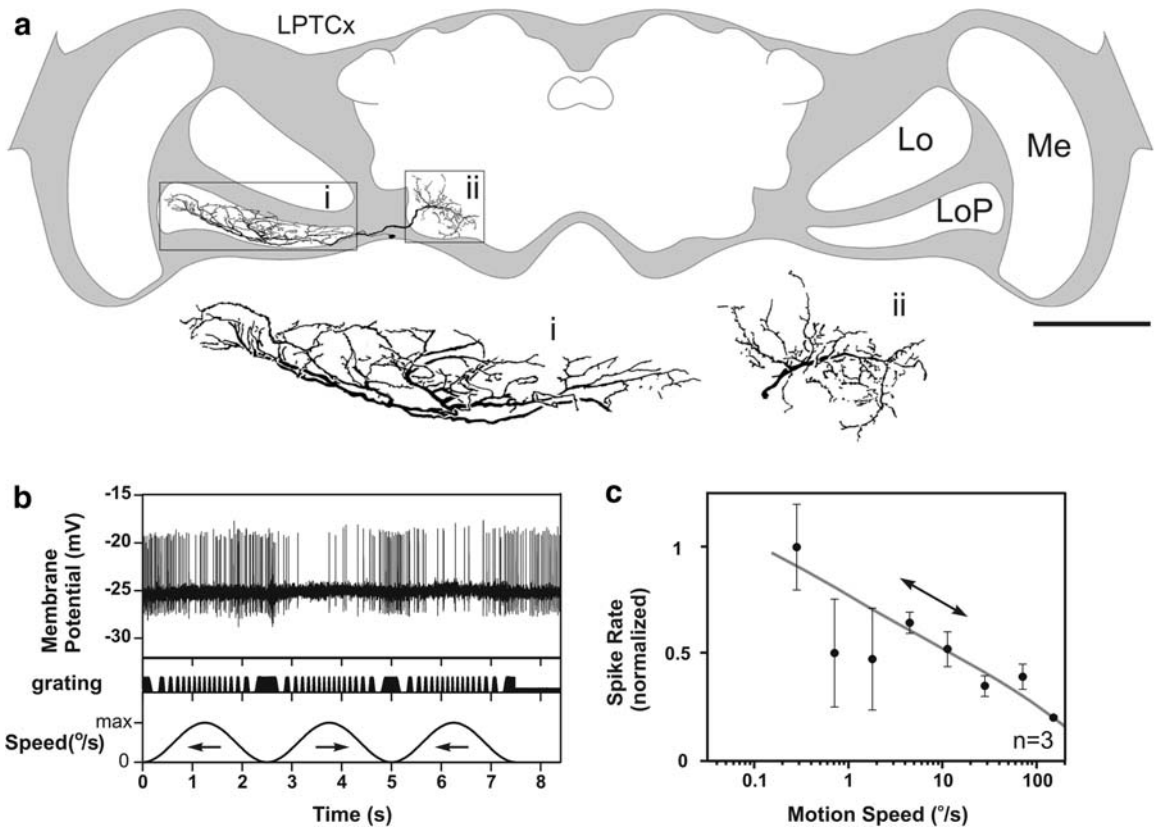

Fig. 2 A previously undescribed wide-field lobula plate tangential neuron (LPTCx), showing background spiking activity that was inhibited by wide-field motion. **a** Horizontal projection of this neuron's morphology in the lobula plate (*LoP*, *inset i*) and in the posterior lateral deutocerebrum (*inset ii*). In the brain outline the lamina and retina have been removed; the head's anterior is toward the top of the page. **b** Motion responses of this neuron soon after penetration, plotted as in Fig. 1 and showing inhibition of background spiking activity by horizontal movement of vertical gratings (0–200°/s; spatial wavelength = 20°. Spiking activity was highest during the periods near $t = 0$, 2.5, 5.0 and 7.5–8.2 s, when motion speed was close to zero. **c** Speed response profile, plotted as in Fig. 1d and showing increased inhibition of the background spiking as motion speed increased (averaged during three velocity cycles of increasing and decreasing speeds). *Arrows* in **b** indicate leftward (progressive) and rightward (regressive) motion. *Lo*, lobula; *LoP*, lobula plate; *Me*, medulla. *Scale bar* in **a** = 100 μm (applies to main figure only)

distinct from those of the other neurons in this study (see below).

We now describe additional speed response profiles from a type 4 bushy T cell (T4), a type 2 centrifugal Y cell (CY2), and the lobula plate tangential neuron H6. Basic response properties of these three neurons have been described (Douglass and Strausfeld 1996), but their responses as a function of motion speed have not previously been examined. Speed response profiles from these three neurons are plotted in Fig. 3. Since the responses of CY2 and H6 were lower during decelerating motion, the data from accelerating and decelerating phases are plotted separately.

Analyses were performed by using responses to motion along the preferred axis of orientation (T4) or in the preferred direction (CY2 and H6). For H6, responses to both the preferred and non-preferred directions are shown to illustrate their close similarity. As these three neurons were nonspiking (T4 and CY2) or produced spikes superimposed on DC voltage shifts (H6), the responses were analyzed by measuring mean voltages per time interval. The results of these analyses reveal distinctive speed response profiles. T4 (Fig. 3a) shows maximal responses at intermediate speed ranges, with little or no difference between the responses to accelerating and decelerating motion. The CY2 neuron (Fig. 3b) is relatively insensitive to low speeds, but shows weak responses to speeds as low as 1°/s and much stronger responses from approximately 40 to at least 100°/s, with its maximum response possibly occurring at higher speeds than those which were tested. H6 (Fig. 3c) shows broad tuning across a nearly 2-log range of speeds from ca. 0.6 to at least 90°/s, and its responses to preferred-direction motion direction are mirrored by those to the non-preferred direction.

Mean speed response profiles of all five neurons are compared in Fig. 4, with error bars omitted for clarity. Four distinct speed response characteristics are clearly

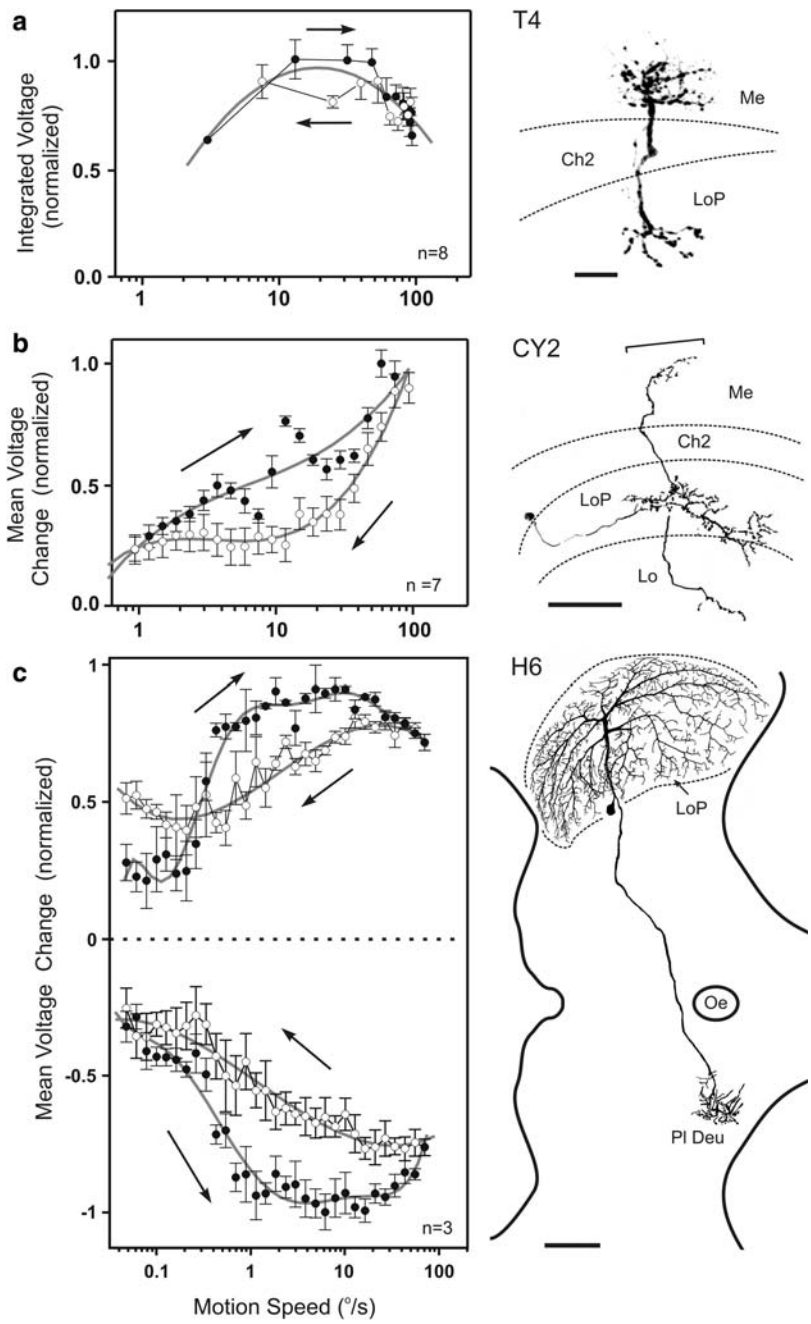

Fig. 3 Normalized responses of three identified optic lobe interneurons (T4, CY2 and H6) as a function of motion speed (mean ± SE), with grating spatial wavelength of 8°. Morphologies of each neuron are illustrated to the right of each plot in horizontal (T4) or vertical (CY2, H6) sections. Responses to accelerating and decelerating motion are shown with *filled* and *open circles*, respectively. and the smooth curves show polynomial fits to the pooled (T4) or separated (CY2 and H6) data. **a** T4 cell, average of eight velocity cycles during horizontal motion, which is the orientation that produced the strongest responses. **b** The centrifugal Y cell CY2; average of seven responses to preferred-direction (*horizontal*) motion. In the illustration of CY2, *bracket* indicates approximately six retinotopic columns in the medulla. **c** The lobula plate tangential cell H6, showing similar speed response profiles during motion in the preferred direction (depolarizations, $n = 3$) and the non-preferred direction (hyperpolarizations, $n = 3$). Individual analyses were designed to be appropriate for the response properties of each neuron (see Materials and methods), including adjustments for response latencies (18, 40 and 50 ms, for T4, CY2 and H6, respectively). The anatomical illustrations are modified after Douglass and Strausfeld (1996). The T4 image was merged from confocal projections; those of CY2 and H6 were hand-drawn from confocal projections. *Dotted lines* indicate approximate borders of neuropils within the optic lobe: *Me* inner medulla, *Ch2* 2nd optic chiasma, *LoP* lobula plate, *Lo* lobula, *Pl Deu* posterolateral deutocerebrum. In **c**, *thick solid lines* indicate outlines of the brain and oesophagus (*Oe*), and the dorsal surface of the brain is to the left. *Scale bars* in **a**, **b** and **c** = 10, 50 and 100 μm, respectively

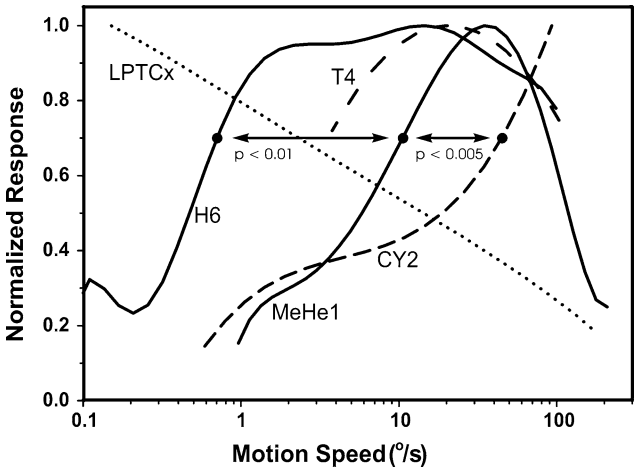

Fig. 4 Comparison of the speed responses of identified fly visual interneurons, showing four distinct speed response profiles. The data are pooled from the best-fit polynomial curves in Figs. 1, 2 and 3. Analysis of motion speeds associated with a 70% maximal response level shows significant differences between H6 and MeHe1 ($P < 0.01$) and between MeHe1 and CY2 ($P < 0.005$; see Results for details). The fitted curves for CY2 and H6 represent only the responses obtained during accelerating motion; responses of these two neurons to decelerating motion were shifted toward slightly higher speeds (see Fig. 3)

discernible: the inhibitory responses of LPTCx, the particularly broad speed range of H6, the intermediate range of T4 and MeHe1, and the sensitivity of CY2 to speeds above the maxima of the other neurons. Visual inspection of the associated error bars (Figs. 1d, 2c, 3) suggests that the differences between speed response profiles are statistically significant. This conclusion is strongly supported by a comparison of the minimum speeds required to obtain criterion response levels from HeMe1, H6 and CY2, as depicted by the filled circles in Fig. 4 for an arbitrarily chosen 70% maximal response level. The LPTCx neuron was omitted from this analysis because its inhibitory responses clearly differ from the other neurons' excitatory responses, and T4 was omitted because insufficient data were available at the relevant speed range. Polynomial fits to the raw speed response profiles from HeMe1, H6 and CY2 were normalized to their respective maxima in order to measure the speeds corresponding to 70% maximal responses. The results of this analysis indicate significant differences between H6 and MeHe1 ($N = 3$ and 8, respectively, Wilcoxon's two-sample test, $P < 0.01$), and between MeHe1 and CY2 ($N = 8$ and 7, respectively, $P < 0.005$).

Selectivity for motion acceleration and deceleration

Whereas the data presented so far are mainly of interest in relation to speed response properties, two additional recordings are suggestive of selectivity for motion acceleration or deceleration. Figure 5a shows a confocal reconstruction of a type of Y cell which has arborizations that reach across several retinotopic columns in the inner medulla. This neuron's spiking activity was short-lived, and the baseline was somewhat unstable, a feature which is not unusual in recordings from small neurons in the fly's optic lobe. The responses nonetheless revealed two important features of this Y neuron's visual filtering properties (Fig. 5b, c). First, the spike rate was low during diagonal downward motion and increased greatly during diagonal upward motion, suggesting a form of directional selectivity. (Additional data showing responses to other motion directions would be needed to clarify the extent of orientation- as opposed to direction-selective tuning; Douglass and Strausfeld 2003a). A second important feature of this recording was evident only during the responses to downward, diagonal motion: the spike rate increased as the motion speed was decreasing (shaded regions in Fig. 5b, c), but not as it was increasing. Thus, in addition to exhibiting strong selectivity for motion direction, a component of this neuron's activity may have been selective for motion deceleration.

Additional evidence for sensitivity to motion acceleration was provided in the second recording (Fig. 6). After an initial brief period of spike-like activity upon impalement, subsequent activity consisted of small, spike-like membrane depolarizations and hyperpolarizations, sometimes accompanied by more sustained hyperpolarizations. In this recording it was possible to test for responses to six different motion directions, as indicated by the arrows in Fig. 6b. Responses occurred only during upward progressive (top 3 panels and bottom panel) and horizontal progressive motion (middle two panels), not during horizontal regressive, downward, or downward-regressive motion. Most importantly, the timing of all of the responses was consistently restricted to periods of motion acceleration (shaded regions). The proportion of responses to acceleration (6 of 6) is significantly different from the proportion of responses to deceleration (0 of 6, $P < 0.001$, Z statistic), suggesting that this neuron was acceleration selective. Because the deceleration phase of each stimulus direction always followed acceleration, however, the periods of inactivity during deceleration could conceivably reflect a particularly rapid form of adaptation to the previous activity.

The neuron corresponding to this recording was either a lobula plate-to-lobula (LLP) neuron (Fig. 6a i and ii) or a transmedullary Y cell (Fig. 6a iii). The approximate position and depth of the recording pipette were known, but it was impossible to determine which of the two stained neurons corresponds to the

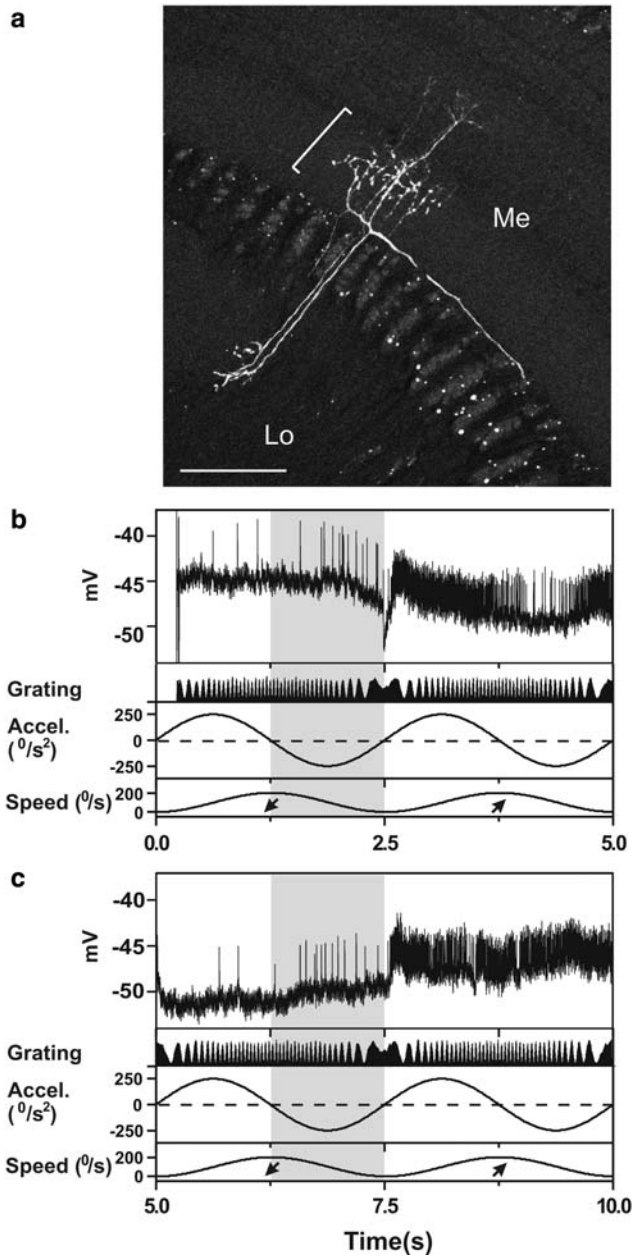

Fig. 5 Inner medulla Y neuron showing activity suggestive of sensitivity to motion deceleration as well as motion direction. **a** Confocal projection showing arbors in the medulla (*Me*) and lobula (*Lo*). **b**, **c** Successive intracellular responses to diagonal grating motion at sinusoidally varied speeds (spatial wavelength = 8°), showing increased spiking during deceleration of downward progressive motion (*shaded*) in both repetitions of the 5 s stimulus sequence. The large voltage fluctuation at the start of the trace in **b** is an artifact of the initial impalement. The slow fluctuations in the baseline appear unrelated to the stimuli. *Scale bar* in **a** = 20 μm

recorded cell. This is because the recording location was in a region between the lobula and lobula plate where the two axons of the stained neurons lie in very close proximity (arrow in Fig. 6a). The axons appear not to have been dye-coupled, as close examination of individual confocal optical sections showed no point of contact.

Discussion

This investigation examined the dynamic response properties of motion-sensitive optic lobe neurons in the fly. The results provide new insight into possible neural mechanisms of speed discrimination in insects. Up to four distinct speed response profiles were observed among medulla and lobula complex neurons, supporting the "multiple STF range" hypothesis as a neural mechanism of speed discrimination in insects. It is also of interest that the fastest tuning observed is to speeds that lie beyond the "blur limit" for blow fly photoreceptors, and that two recordings were suggestive of acceleration selectivity. These latter observations underscore the need for additional research concerning the extent to which dynamic and rapidly changing motion inputs are processed in the fly's visual system.

Factors that could affect the accuracy of the speed response profiles

A common feature of intracellular recordings from small optic lobe interneurons is that membrane potentials and response amplitudes may become unstable within a few minutes of impalement. Thus, in this investigation it was not possible to test responses to more than one spatial wavelength. But since all but the inhibitory LPTCx neuron were subjected to the same 0.126 cpd stimulus, their responses are directly comparable. Though the recordings also comprise a small sample of neurons, all of the response properties described here were observed consistently upon repeated stimulation.

As visual stimuli, sinusoidally modulated motion speeds (e.g., Egelhaaf and Reichardt 1987; Cao et al. 2004) have specific advantages and disadvantages. They are useful for observing responses across a broad range of speeds and include an acceleration component, while avoiding potentially artifactual responses to the sudden discontinuities at the beginning and end of a constant-speed stimulus. Although response levels at a given time interval are not independent of preceding stimulus conditions, studies using randomly modulated speeds suggest that the use of dynamic speed modulations can actually increase the coherence between stimulus velocities and responses (Haag and Borst 1997). Finally, if there is a significant latency in

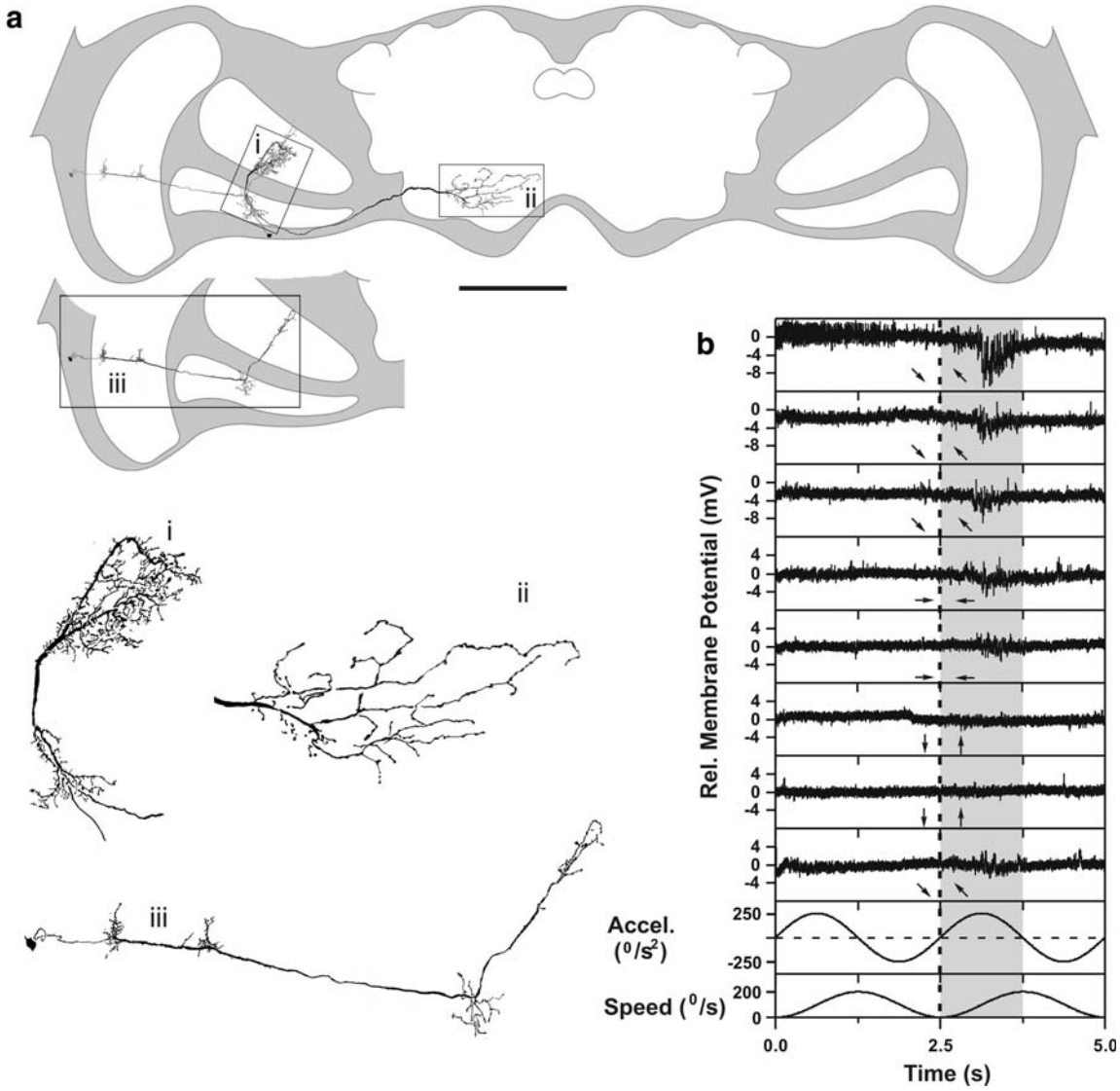

Fig. 6 Lobula-to-lobula plate (*LLP*) and small-field columnar Y cell, both of which were stained near the time of this recording (see text for details). **a** Brain overviews show the approximate locations of the neurons in the optic lobe and the position of the recording pipette (*arrow*). Insets show details of the LPL neuron (*i and ii*) and the Y neuron (*iii*, with repeated brain background to show relationships with medulla, lobula and lobula plate). **b** Grating motions were presented at sinusoidally varied speeds in six directions (along three axes of orientation). The recording is plotted relative to the initial resting membrane potential of ca. −15 mV, and shows a chronological sequence of responses to 16 velocity and acceleration cycles. All responses occurred during accelerating (*shaded*), upward-progressive or horizontal-progressive motion. Individual panels show successive responses to downward regressive followed by upward progressive motion (*top three panels*), regressive then progressive horizontal motion (*fourth and fifth panels*), downward then upward motion (*sixth and seventh panels*), and finally, a fourth repetition of the initial diagonal stimuli (*eighth panel*). *Bottom two panels* indicate the grating speed and acceleration magnitudes, as in Fig. 5. Grating spatial wavelength = 8°; *scale bar* in **a** (main figure only) = 100 μm

the response of a neuron to the instantaneous speed, this could shift its apparent speed sensitivity accordingly. As noted in the Materials and methods, however, such an effect should be small relative to the duration of velocity sweeps, and was further minimized by incorporating the measured response latencies of 18–50 ms into the speed response analyses.

Could differing levels of motion adaptation account for some of the observed variability in speed response profiles? In the lobula plate tangential neuron H1, motion adaptation occurs at high contrast frequencies within seconds of the start of a constant-speed motion stimulus (Maddess and Laughlin 1985). As previously mentioned, the gradual reduction in background spiking of the LPTCx neuron may also reflect motion adaptation. But if so, additional adaptation of LPTCx would only shift the speed response curve toward slower speeds, further accentuating its distinctness from the

other profiles in Fig. 4. In other preparations that were analyzed for speed responses the overall activity levels were much more stationary, perhaps in part because prior exposure of the preparation to sinusoidal motion stimulation as the pipette was advanced into the tissue produced some motion preadaptation. A different type of adaptation is evident in the recordings from CY2 and H6 (Fig. 3), where overall responsiveness was stable, yet hysteresis was evident in the sensitivity to accelerating and decelerating motion. In Fig. 4, the curves derived from these two neurons represent only the responses during acceleration. During deceleration (Fig. 3), the speed response profiles of both neurons were shifted toward slightly higher speed ranges, bringing the H6 speed range closer to those of T4 and HeMe1, and the CY2 range farther from them. In summary, effects of motion adaptation appear to be relatively small compared to the observed differences in speed response profiles.

Another possible source of variability in the speed response profiles was already introduced in the Methods, where it is shown that the maximum geometric distortions of apparent stimulus speeds were small compared to the full range of speeds that are plotted in Figs. 3 and 4. Consideration of the spatial receptive fields of individual neurons (when known), or alternatively the retinotopic position of their dendritic fields, suggests that actual discrepancies in apparent speeds were even smaller. During the T4 cell recording, stimulation with a small-field, mobile flicker stimulus revealed its receptive field approximately 15–20° rightward and upward from the center of the display (data not shown). Although receptive field data are not available for MeHe1 and CY2, their dendritic field positions (see Fig. 1 and Douglass and Strausfeld 1996, respectively) are also indicative of receptive field locations that were only slightly displaced from the center of the display. As the dendritic fields of the wide-field neurons H6 and LPTC extend across the entire lobula plate, they were stimulated by the full area of the CRT stimulus, resulting in a mean variation in apparent log speed of less than 0.3. Thus, although geometric distortions in apparent speeds could indeed have shifted the relative positions of the measured speed response profiles, such effects appear to be insufficient to alter the overall findings that are further discussed below.

Distinct speed responses indicate multiple spatiotemporal tunings

The results show for the first time that motion sensitive neurons that arborize in the inner medulla and in the lobula complex exhibit up to four distinct speed response tuning ranges. Since tests of each neuron were performed with a single grating spatial frequency (0.13 cpd in all but one case), it was not possible to evaluate whether these neurons are themselves speed-*selective* to grating motion. Nevertheless, because the single-spatial-frequency data (Fig. 4) show multiple speed response profiles with distinct speed maxima, this strongly suggests the presence of distinct overall STF tunings, as illustrated schematically in Fig. 7a for three hypothetical neurons. This observation thus supports the plausibility of a "multiple STF range" mechanism of generating speed selectivity, in which activity levels of relatively unspecialized STF-tuned neurons (Fig. 7a) are compared (Fig. 7b) to yield tuning that is more speed-selective(Fig. 7c).

The H6 neuron responds strongly across a 2-log-unit range of relatively low speeds, T4 and MeHe1 respond

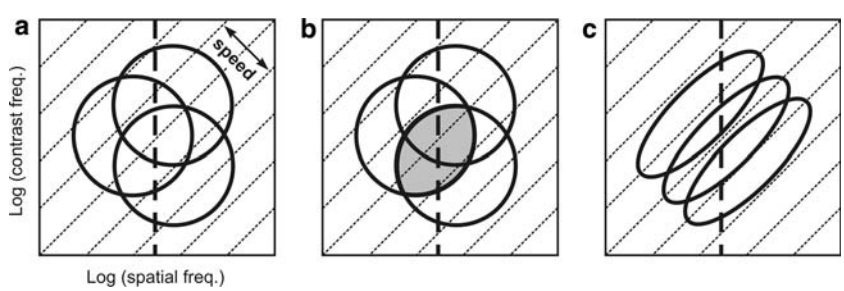

Fig. 7 Schematic plots depicting spatiotemporal response profiles of hypothetical motion sensitive neurons stimulated with moving gratings across a range of spatial frequencies (abscissa, in cycles/degree, increasing from left to right) and contrast frequencies (ordinate; in cycles/s, increasing toward top of page). The *dashed diagonal lines* show isospeed contours, with speeds increasing from the lower right to upper left corner of each plot. (See Introduction for an equation relating contrast frequency and spatial frequency to speed). **a** Supposing a population of motion-sensitive neurons that are equally affected by speed versus contrast frequency, distinct speed response profiles exhibited by individual neurons tested at a single spatial frequency (*vertical dashed line*) reflect distinct overall spatiotemporal tunings. **b** A hypothetical circuit that compares responses (*shaded region*) of non-speed-selective neurons thus could generate speed-selective activity at a subsequent processing level, as illustrated for three speed-selective neurons in (**c**)

to intermediate speeds, CY2 responds best to high speeds, and LPTCx, in common with previously described lobula plate tangentials termed CH (Hausen 1984), is inhibited by motion. These results suggest either that these neurons are supplied by several emd types having distinct STF tuning ranges, or that the outputs of a single class of very broadly tuned emds are selectively filtered to produce the observed tuning ranges. Regardless of the precise mechanisms of generating speed selectivity, the mere presence of distinct speed-response profiles suggests that even animals with small brains can afford to devote separate subsets of neurons to distinct portions of the spatiotemporal tuning landscape.

The observation of multiple speed response profiles from only a few neurons brings up interesting questions regarding how many distinct STF ranges are present in the fly's visual system, and how many would be suitable for a particular speed discrimination task. If constraints on brain size impose strict limits on the maximum number of STF ranges that can be represented, it would seem unexpected to find such diversity in such a small sample. Yet in general, sensory tuning ranges of individual neurons in arthropods may either be widely distributed across a given parameter range, or tightly clustered. Examples of a diversity of tuning ranges and maxima include the preferred directions of wind-sensitive hairs on cricket cerci (Landolfa and Jacobs 1995) and the specificities of insect olfactory receptors (e.g., Couto et al. 2005). Where there is tighter clustering around a few types, as in the spectral sensitivities of photoreceptors (Osorio and Vorobyev 2005), such clustering may reflect constraints which are unrelated to computational demands. If the STF tunings of motion-sensitive neurons in the fly's medulla and lobula neuropils are diverse and not tightly clustered, then our observed speed response profiles would not be unexpected. Still, the current data clearly provide only a glimpse of overall STF tuning properties, and it will be of considerable interest if future investigations can achieve more complete characterizations of STF tuning in a larger sample of identified neurons.

Suggested pathways for processing slower and faster motion

There is some evidence for distinct speed response ranges in insect visual interneurons at the level of descending neurons (DNs) in blow flies, locusts and butterflies. DNs relay information from visual as well as other sensory modalities, from the central brain to thoracic neuropils that control wing and leg muscles (Gronenberg et al. 1995). Using a grating spatial wavelength of 11.5° (closely comparable to our 8° grating), Horridge and Marcelja (1992) distinguished peak responses of "slow" DNs, near 50°/s, from those of "fast" DNs (ca. 150–250°/s). Also included among "slow" neurons in the fly were extracellular recordings attributed to the H1 neuron in the lobula plate (Horridge and Marcelja 1992). The current results suggest a preliminary conception of the types of neural pathways that may selectively relay information about slower versus faster motion to these subsets of descending neurons.

In addition to possible inputs from H1, the speed responses of Horridge and Marcelja's (1992) "slower" DNs could reflect inputs from neurons like HeMe1 (Fig. 1) and H6 (Fig. 3d), both of which supply terminal arborizations in circumscribed neuropils of the dorsolateral deutocerebrum that are associated with DNs supplying flight motor neuropil (Strausfeld and Gronenberg 1990). Inputs to those lobula plate efferent neurons that supply slower DNs might, in turn, include the endings of T4 cells in the lobula plate. The possible outlines of a pathway to "faster" DNs are less apparent, but could include CY2 neurons. As DNs do not extend their dendrites to the lobula levels where the terminals of CY2 reside, at least one additional relay element would be needed to connect DN dendrites in the protocerebrum with CY2 endings in the lobula. Possible candidate relays are provided by a variety of retinotopic lobula outputs that project to the optic foci, known as lobula-plate-to-lobula neurons (LPLs; Strausfeld and Gilbert 1992; Gilbert and Strausfeld 1992) and lobula projection neurons.

Possible functional implications of sensitivity to high speeds and to acceleration

The speed response profile of CY2 peaked at 200°/s (Fig. 3b), which suggests that the true maximum response may lie at a higher speed. Peak responses at from 150 to 200°/s also have been observed in descending neurons, not only in the dragonfly *Anax*, a fast visual predator (8° grating period; Olberg 1981), but also in the blow fly *Calliphora* (11.5° grating; Horridge and Marcelja 1992). Yet, according to theoretical predictions (Srinivasan and Bernard 1975; Land 1999) as well as photoreceptor and monopolar cell recordings from blow flies (Juusola and French 1997), significant blurring of the retina's responses to a moving scene begins at angular velocities above approximately 200°/s. When angular velocities exceed the theoretical blur limit for the retina, how can interneurons still transmit meaningful visual information? As Olberg (1981) pointed out, this is possible if spatial

resolution is sacrificed for increased temporal resolution. As the dendritic field of CY2 in the lobula plate spans a region equivalent to several retinal visual sampling units, its input organization appears well-suited for possibly increasing the effective blur limit in this manner.

Using a combination of sinusoidally-modulated and constant-acceleration visual stimuli, Cao et al. (2004) discovered neurons in the pigeon's pretectal nucleus which are particularly sensitive to acceleration and deceleration. This suggests that in addition to analyzing direction and speed information, visual motion-processing pathways may also exploit visual acceleration information. Indeed, studies of theoretical motion detectors have predicted that movement detector responses to dynamic stimuli can be affected not only by velocity, but also by acceleration as well as higher-order velocity derivatives (Egelhaaf and Reichardt 1987). Are actual insect visual interneurons influenced by acceleration, and if so, is this activity functionally significant? In the lobula plate of the fly, strong transient responses of the H1 cell to the sudden onset of constant-speed motion (Egelhaaf and Borst 1989) hint at acceleration sensitivity, but with this stimulus the acceleration component is virtually instantaneous and coincides with the onset of motion, so the transient activity could simply reflect a rapidly adapting response to the sudden onset of a constant velocity. In recordings employing sinusoidally modulated grating motion, interpretation of responses is less problematic because the time courses of velocity and acceleration are phase shifted, the peaks in velocity corresponding to zero acceleration. When stimulated with sinusoidal motion at high contrast frequencies, responses of the HSS neuron included a component that was correlated with acceleration (Egelhaaf and Reichardt 1987), but the time course of the overall response pattern was complex.

Here, two additional recordings from identified neurons offer further support of a possible role for acceleration processing in insects. Although deceleration selectivity is not the only possible explanation for the subtle correlation noted in Fig. 5, it is one of perhaps two plausible explanations. In the second recording (Fig. 6), the correlation of the observed activity with acceleration is statistically significant, and sensitivity to acceleration appears to be the most parsimonious interpretation. In future investigations of possible acceleration-selective activity, it will be useful to employ additional stimuli which are designed specifically to uncover responses to acceleration, including both sinusoidally-modulated and constant accelerations (cf. Cao et al. 2004).

Acknowledgments We thank Drs. Wulfila Gronenberg, Charles M. Higgins and two anonymous reviewers for helpful discussions and critical comments on the manuscript. This work was supported by NIH 5 R01 RR008688-17. The experiments complied with the current laws of the United States and with "Principles of animal care", publication No. 86-23, revised 1985 of the National Institutes of Health.

References

Borst A, Egelhaaf M (1989) Principles of visual motion detection. Trends Neurosci 12(8):297–306

Cao P, Gu Y, Wang SR (2004) Visual neurons in the pigeon brain encode the acceleration of stimulus motion. J Neurosci 24(35):7690–7698

Couto A, Alenius M, Dickson BJ (2005) Molecular, anatomical, and functional organization of the *Drosophila* olfactory system. Curr Biol 15:1535–1547

David CT (1982) Compensation for height in the control of groundspeed by *Drosophila* in a new, "Barber's Pole" wind tunnel. J Comp Physiol 147:485–493

Douglass JK, Strausfeld NJ (1996) Visual motion-detection circuits in flies: parallel direction- and non-direction-sensitive pathways between the medulla and lobula plate. J Neurosci 16:4551–4562

Douglass JK, Strausfeld NJ (1998) Functionally and anatomically segregated visual pathways in the lobula complex of a calliphorid fly. J Comp Neurol 396:84–104

Douglass JK, Strausfeld NJ (2003a) Anatomical organization of retinotopic motion-sensitive pathways in the optic lobes of flies. Microsc Res Techn 62:132–150

Douglass JK, Strausfeld NJ (2003b) Retinotopic pathways providing motion-selective information to the lobula from peripheral elementary motion-detecting circuits. J Comp Neurol 457:326–344

Dror RO, O'Carroll DC, Laughlin SB (2001) Accuracy of velocity estimation by Reichardt correlators. J Opt Soc Am A Opt Image Sci Vis 18:241–252

Eckert H (1980) Functional properties of the H1 neuron in the third optic ganglion of the blowfly *Phaenicia*. J Comp Physiol 135:29–39

Egelhaaf M, Borst A (1989) Transient and steady-state response properties of movement detectors. J Opt Soc Am A 6:116–127

Egelhaaf M, Reichardt W (1987) Dynamic response properties of movement detectors: theoretical analysis and electrophysiological investigation in the visual system of the fly. Biol Cybern 56:69–87

Gilbert C, Strausfeld NJ (1992) Small-field neurons associated with oculomotor and optomotor control in muscoid flies: functional organization. J Comp Neurol 316:72–86

Gronenberg W, Milde JJ, Strausfeld NJ (1995) Oculomotor control in calliphorid flies: organization of descending neurons to neck motor neurons responding to visual stimuli. J Comp Neurol 361:267–284

Grzywacz NM, Yuille AL (1990) A model for the estimate of local image velocity by cells in the visual cortex. Proc R Soc Lond B 239:120–161

Haag J, Borst A (1997) Encoding of visual motion information and reliability in spiking and graded potential neurons. J Neurosci 17:4809–4819

Hassenstein B, Reichardt W (1956) Systemtheoretische Analyse der Zeit-, Reihenfolgen- unt Vorzeichenauswertung bei der Bewegungsperzeption des Rüsselkäfers *Chlorophanus*. Z Naturforsch 11:513–524

van Hateren JH (1997) Processing of natural time series of intensities by the visual system of the blowfly. Vision Res 37: 3407–3416

Hausen K (1984) The lobula complex of the fly: structure, function and significance in visual behavior. In: Ali MA (ed) Photoreception and vision in invertebrates. Plenum, New York, pp 523–599

Higgins CM (2004) Nondirectional motion may underlie insect behavioral dependence on image speed. Biol Cybern 91:326–332

Higgins CM, Douglass JK, Strausfeld NJ (2004) The computational basis of an identified neuronal circuit for elementary motion detection in dipterous insects. Visual Neurosci 21:567–586

Horridge GA, Marcelja L (1992) On the existence of 'fast' and 'slow' directionally sensitive motion detector neurons in insects. Proc R Soc Lond B 248:47–54

Ibbotson MR (2001) Evidence for velocity-tuned motion-sensitive descending neurons in the honeybee. Proc R Soc Lond B 268:2195–2201

Juusola M, French AS (1997) Visual acuity for moving objects in first- and second-order neurons of the fly compound eye. J Neurophysiol 77:1487–1495

Kien J (1975) Neuronal mechanisms subserving directional selectivity in the locust optomotor system. J Comp Physiol 102:337–355

Land MF (1999) Motion and vision: why animals move their eyes. J Comp Physiol A 185(4):341–352

Landolfa MA, Jacobs GA (1995) Direction sensitivity of the filiform hair population of the cricket cercal system. J Comp Physiol A 177:759–766

Maddess T, Laughlin SB (1985) Adaptation of the motion-sensitive neuron H1 is generated locally and governed by contrast frequency. Proc R Soc Lond B 225:251–275

Meinertzhagen IA, Hanson TA (1993) The development of the optic lobes. In: Bate M, Arias AM (eds) The development of *Drosophila melanogaster*. Cold Spring Harbour Laboratory Press, Cold Spring Harbour, pp 1363–1490

O'Carroll DC, Bidwell NJ, Laughlin SB, Warrant EJ (1996) Insect motion detectors matched to visual ecology. Nature 382:63–66

O'Carroll DC, Laughlin SB, Bidwell NJ, Harris RA (1997) Spatio-temporal properties of motion detectors matched to low image velocities in hovering insects. Vision Res 37: 3427–3439

Olberg RM (1981) Object- and self-movement detectors in the ventral nerve cord of the dragonfly. J Comp Physiol 141:327–334

Osorio D, Vorobyev M (2005) Photoreceptor spectral sensitivities in terrestrial animals; adaptations for luminance and colour vision. Proc Biol Sci 272:1745–1752

Perrone JA, Thiele A (2001) Speed skills: measuring the visual speed analyzing properties of primate MT neurons. Nat Neurosci 4:526–532

Priebe NJ, Lisberger SG, Movshon JA (2006) Tuning for spatiotemporal frequency and speed in directionally selective neurons of macaque striate cortex. J Neurosci 26:2941–2950

Shoemaker PA, O'Carroll DC and Straw AD (2005) Velocity constancy and models for wide-field visual motion detection in insects. Biol Cybern 93:275–287

Sokal RR, Rohlf FJ (1981) Biometry, 2nd edn. W.H. Freeman & Co., New York, p 859

Srinivasan MV, Bernard G (1975) The effect of motion on visual acuity of the compound eye: a theoretical analysis. Vision Res 15:515–525

Srinivasan MV, Lehrer M, Kirchner WH, Zhang SW (1991) Range perception through apparent image speed in freely flying honeybees. Vis Neurosci 6:519–535

Srinivasan M, Zhang S, Lehrer M, Collett T (1996) Honeybee navigation en route to the goal: visual flight control and odometry. J Exp Biol 199:237–244

Srinivasan MV, Zhang SW, Chahl JS, Barth E, Venkatesh S (2000) How honeybees make grazing landings on flat surfaces. Biol Cybern 83:171–183

Strausfeld NJ (1991) Structural organization of male-specific visual neurons in calliphorid optic lobes. J Comp Physiol A 169:379–393

Strausfeld NJ (2005) The evolution of crustacean and insect optic lobes and the origins of chiasmata. Arthropod Struct Dev 34:235–256

Strausfeld NJ, Gilbert C (1992) Small-field neurons associated with oculomotor and optomotor control in muscoid flies: cellular organization in the lobula plate. J Comp Neurol 316:56–71

Strausfeld NJ, Gronenberg W (1990) Descending neurons supplying the neck and flight motor of Diptera: organization and neuroanatomical relationships with visual pathways. J Comp Neurol 302:954–972

Strausfeld NJ, Lee J-K (1991) Neuronal basis for parallel visual processing in the fly. Visual Neurosci 7:13–33

Streidter GF (2005) Principles of brain evolution. Sinauer Associates, Sunderland

Walpole RE (1974) Introduction to statistics. The Macmillan Co., New York, 340 pp

Zanker JM, Srinivasan MV, Egelhaaf M (1999) Speed tuning in elementary motion detectors of the correlation type. Biol Cybern 80:109–116